

# Network-Forming Units, Energy Landscapes, and Conductivity Activation Energies in Alkali Borophosphate Glasses: Analytical Approaches

Marco Bosi, Julian Fischer, and Philipp Maass\*

*Universität Osnabrück, Fachbereich Physik, Barbarastrasse 7, D-49076 Osnabrück, Germany*

E-mail: maass@uni-osnabrueck.de

## Abstract

A major challenge in the modeling of ionically conducting glasses is to understand how the large variety of possible chemical compositions and specific features of their structure influence ionic transport quantities. Here we revisit and extend a theoretical approach for alkali borophosphate glasses, where changes of conductivity activation energies with the borate to phosphate mixing ratio are related to modifications of the ionic site energy landscape. The landscape modifications are caused by varying amounts of different units forming the glassy network, which lead to spatial redistributions of the counter-charges of the mobile alkali ions. Theoretical approaches are presented to calculate variations of both network former unit concentrations and activation energies with the glass composition. Applications to several alkali borophosphate glasses show good agreement with experimental data.

## 1 Introduction

High ionic conductivities are desired when optimizing glassy electrolytes for most applications.<sup>1</sup> To guide this optimization process, it is important to improve our theoretical understanding of ion motion in glasses.<sup>2</sup> Strong enhancements of ionic conductivities can be achieved by utilizing various effects, which we term the “ionic concentration effect”, “halide

doping effect”, and “mixed glass former effect”. For the ionic concentration effect, a strong (superlinear) increase of ionic conductivity results from an increase of the molar content of mobile ions,<sup>3</sup> and for the halide doping effect from an addition of alkali halides.<sup>4</sup> In the case of the “mixed glass former effect”,<sup>5,6</sup> a mixing of different types of glass formers, such as silicates, borates, phosphates etc., can lead to a conductivity increase at intermediate mixing ratios. Different theoretical approaches were developed to understand underlying physical mechanisms causing the ionic concentration,<sup>7–10</sup> the halide doping<sup>11</sup> and the mixed glass former effect (MGFE).<sup>12–14</sup>

The MGFE received particular attention in the last decade.<sup>13,15</sup> Upon mixing of two or more glass formers, the ionic conductivity can increase (positive MGFE)<sup>16</sup> or decrease (negative MGFE).<sup>17,18</sup> Many studies in particular were conducted for alkali borophosphate glasses.<sup>14,19–22</sup>

In a former study, our research group developed a theoretical approach to explain the MGFE in sodium borophosphate glasses with compositions  $0.4\text{Na}_2\text{O}-0.6[x\text{B}_2\text{O}_3-(1-x)\text{P}_2\text{O}_5]$  in the whole range of borate to phosphate mixing  $0 \leq x \leq 1$ .<sup>14</sup> In this approach, a thermodynamical model was first introduced to describe how relative amounts of different types of network forming units (NFUs) change with  $x$ . Excellent agreement with experimental results from magic angle spinning nuclear magnetic

resonance (MAS NMR) was obtained. Based on the NFU concentrations, energy landscapes for the sodium ion migration were constructed, and the ionic transport studied by extensive kinetic Monte Carlo (KMC) simulations. These simulations allowed the extraction of activation energies from Arrhenius plots of long-time sodium diffusion coefficients. The variation of the activation energies with  $x$  showed good agreement with experimental results for conductivity activation energies obtained from impedance spectroscopy. Only one disorder parameter was fitted in the theory, when assuming a given concentration of vacant ionic sites in the glass network. This parameter specifies additional fluctuations in the energetics of individual ion jumps.

Here we revisit the theoretical approach and give explicit expressions for the NFU concentrations, including additional results in the case of low alkali concentrations. Thereafter we show that it is possible to calculate conductivity activation energies analytically from the landscape construction, which compare well with the KMC results and experimental data.

We first discuss that evaluating differences between percolation and Fermi energies, as suggested earlier,<sup>10,23,24</sup> yields approximate results only. An accurate theory is provided by an effective mapping to a disordered conductance network,<sup>25,26</sup> or equivalently, to a single-particle hopping model in a landscape with spatially varying jump barriers. This means that a purely analytical approach, with just a numerical determination of Fermi energies and critical percolation barriers, is able to connect information on the structure (NFU concentrations) with transport properties (activation energies) in very good agreement with experiments. We find it surprising that this is possible in a complex disordered system such as the sodium borophosphate glasses.

The analytical treatment allows avoiding extensive computer simulations and for checking the robustness of the theoretical approach against variations of parameters within reasonable limits, in particular the concentration of vacant ionic sites. Moreover, one can quickly apply the approach now to other

borophosphate glasses. We demonstrate this for lithium borophosphate glasses with compositions  $0.33\text{Li}_2\text{O}-0.67[x\text{B}_2\text{O}_3-(1-x)\text{P}_2\text{O}_5]$ , where experimental results for NFU concentrations and activation energies were reported in Ref. 27.

## 2 Network Former Unit Concentrations

MAS-NMR studies for borophosphate glasses<sup>20,28</sup> with compositions  $y\text{M}_2\text{O}-(1-y)[x\text{B}_2\text{O}_3-(1-x)\text{P}_2\text{O}_5]$  ( $M$ : alkali ion,  $y$ : molar fraction of alkali oxide) have shown the occurrence of eight different NFU types, see Fig. 1: neutral trigonal  $\text{B}^{(3)}$  units with three bridging oxygens (bOs), trigonal  $\text{B}^{(2)}$  units with two bOs and one negatively charged nonbridging oxygen (nbO), negatively charged tetrahedral  $\text{B}^{(4)}$  units with four bOs, and tetrahedral phosphate units  $\text{P}^{(n)}$ ,  $n = 0, \dots, 4$ , with  $n$  bOs,  $(4-n)$  nbOs, and charges  $(n-3)$  (in units of the elementary charge). The concentration of these different NFU types depends on the overall glass composition.

We denote by  $\{X\}$  ( $X = \text{B}^{(n)}$ ,  $n = 2, 3, 4$ , or  $\text{P}^{(n)}$ ,  $n = 0, \dots, 4$ ) the fraction of NFUs with

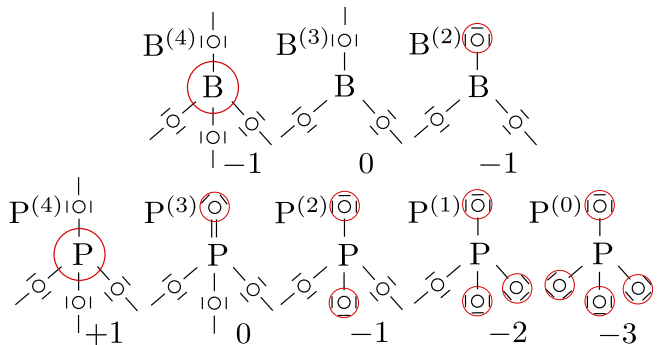


Figure 1: Sketches of the different NFUs forming a network in borophosphate glasses. The upper and lower rows show the  $\text{B}^{(n)}$  and  $\text{P}^{(n)}$  units with  $n$  bridging oxygens, respectively. The numbers indicate the charges of the species (in units of the elementary charge) and the red circles illustrate how the total charge can be viewed as (partially) distributed among nonbridging oxygens or among all oxygens in the absence of nonbridging ones.

**Table 1: Theoretically predicted fractions of the number of NFUs of different types relative to the total number of NFUs in alkali borophosphate glasses of compositions  $yM_2O \cdot (1-y)[xB_2O_3 \cdot (1-x)P_2O_5]$  with  $y \geq 3/10$  ( $\{M\} = y/(1-y) \geq 3/7$ ). The NFU fractions exhibit different dependencies on the alkali ion fraction  $\{M\} = y/(1-y)$  in various regimes of the borate to phosphate mixing ratio  $x$ . The borders of the different regimes are given by  $x_1 = (9 - \{M\})/20$ ,  $x_2^I = (29 - 21\{M\})/20$ ,  $x_2^{II} = (45 - 21\{M\})/36$ , and  $x_2 = 7/6 - 7\{M\}/18$ .**

NFU	$0 \leq x \leq x_1$	$x_1 \leq x \leq x_2^I$	$x_2^I \leq x \leq x_2^{II}$	$x_2^{II} \leq x \leq x_2$	$x_2 \leq x \leq 1$
B <sup>(2)</sup>	0	0	0	0	$\frac{-21+7\{M\}}{6} + 3x$
B <sup>(3)</sup>	0	$-\frac{9-\{M\}}{20} + x$	$\frac{-13+5\{M\}}{16} + \frac{5}{4}x$	$-\frac{3-\{M\}}{6} + x$	$3-\{M\}-2x$
B <sup>(4)</sup>	$x$	$\frac{9-\{M\}}{20}$	$\frac{13-5\{M\}}{16} - \frac{1}{4}x$	$\frac{3-\{M\}}{6}$	$\frac{3-\{M\}}{6}$
P <sup>(0)</sup>	0	0	0	$\frac{-15+7\{M\}}{6} + 2x$	$1-x$
P <sup>(1)</sup>	0	0	$\frac{-29+21\{M\}}{16} + \frac{5}{4}x$	$\frac{21-7\{M\}}{6} - 3x$	0
P <sup>(2)</sup>	$\{M\}-x$	$\frac{-9+21\{M\}}{20}$	$\frac{45-21\{M\}}{16} - \frac{9}{4}x$	0	0
P <sup>(3)</sup>	$1-\{M\}$	$\frac{29-21\{M\}}{20} - x$	0	0	0

respect to the network forming cations, *i.e.*

$$\{X\} = \frac{[X]}{[B] + [P]} \quad (1)$$

The molar fractions are  $[X] = ([B] + [P])\{X\} = (1-y)\{X\}$ . The total boron content, the total phosphorus content, and the charge neutrality give the following constraints:

$$\sum_{n=2}^4 \{B^{(n)}\} = x, \quad (2a)$$

$$\sum_{n=0}^4 \{P^{(n)}\} = (1-x), \quad (2b)$$

$$\begin{aligned} \{B^{(4)}\} + \{B^{(2)}\} + \{P^{(2)}\} + 2\{P^{(1)}\} + 3\{P^{(0)}\} \\ = \{M\} + \{P^{(4)}\}, \end{aligned} \quad (2c)$$

where

$$\{M\} = \frac{y}{1-y}. \quad (3)$$

Equations (2a)-(2c) are three determining equations for the eight unknown NFU fractions.

To obtain a complete set of determining equations, a thermodynamic model was developed,<sup>14</sup> which is based on different formation enthalpies  $G_X$  of the NFUs  $X$ . The differences between these formation enthalpies can be related to the charge delocalization in the NFUs, with lower formation enthalpies for higher delocalization.

If differences  $\Delta G_X$  are significantly larger than the thermal energy  $k_B T_g$  at the glass transition ( $T_g$ : glass transition temperature), a hierarchy results with respect to the preference of the negatively charged NFUs to compensate for the alkali ion charges. In the absence of

**Table 2: Theoretically predicted NFU fractions as in Table 1 for  $y \leq 3/10$  ( $\{M\} = y/(1-y) \leq 3/7$ ). The borders of the different regimes are given by  $x_1 = \{M\}$ ,  $x_2 = (3 - \{M\})/6$ , and  $x_3 = (3 + 7\{M\})/6$ , see Eqs. (6), (8), and (10).**

NFU	$0 \leq x \leq x_1$	$x_1 \leq x \leq x_2$	$x_2 \leq x \leq x_3$	$x_3 \leq x \leq 1$
B <sup>(3)</sup>	0	0	$-\frac{3 - \{M\}}{6} + x$	$-1 - \{M\} + 2x$
B <sup>(4)</sup>	$x$	$x$	$\frac{3 - \{M\}}{6}$	$1 + \{M\} - x$
P <sup>(2)</sup>	$\{M\} - x$	0	0	0
P <sup>(3)</sup>	$1 - \{M\}$	$1 + \{M\} - 2x$	$\frac{3 + 7\{M\}}{6} - x$	0
P <sup>(4)</sup>	0	$-\{M\} + x$	$\frac{3 - 7\{M\}}{6}$	$1 - x$

P<sup>(4)</sup> units, which were not considered in Ref. 14, the hierarchy corresponds to an ordering  $G_{B^{(4)}} < G_{P^{(2)}} < G_{P^{(1)}} < G_{P^{(0)}} < G_{B^{(2)}}$  of the charged NFU types. The hierarchy implies that NFU types with higher formation enthalpy do not occur unless they must form to satisfy all constraints. In addition to the constraints given by the equations (2a)-(2c), an important further one is that of forbidden linkages between B<sup>(4)</sup> units.<sup>30</sup> This can be attributed to the homogeneously delocalized charge of the B<sup>(4)</sup> units, which impedes the formation of an oxygen bridge between them. For small  $\Delta G_X$ , which are less than about  $4k_B T_g$ , it is possible to refine the treatment by introducing disproportionation reactions between the respective NFU types.

In Table 1 we give the fractions  $\{X\}$  of the various NFU types predicted by the theory<sup>14</sup> without consideration of disproportionation reactions, and for alkali ion fractions  $\{M\}$  larger than a critical value  $\{M\}_* = 3/7 \cong 0.43$ . In this regime of high alkali content, we predict no P<sup>(4)</sup> units to occur (see below). Using the equations in Table 1, we find good agreement with MAS-NMR results for various series of alkali borophosphate glasses with compositions  $0.4\text{Na}_2\text{O}-0.6[x\text{B}_2\text{O}_3-(1-x)\text{P}_2\text{O}_5]$ ,  $y\text{Na}_2\text{O}-$

$2(1-y)[\text{BPO}_4]$ , and  $0.33\text{Li}_2\text{O}-0.67[x\text{B}_2\text{O}_3-(1-x)\text{P}_2\text{O}_5]$ , see Fig. 2.

If  $\{M\}$  is smaller than  $\{M\}_* = 3/7$  (or  $y = \{M\}/(1 + \{M\}) < 0.3$ ), one needs to consider the P<sup>(4)</sup> units also. This NFU type has not been considered in Ref. 14, but experimental observations give strong evidence of its occurrence.<sup>28,31</sup> At low alkali content, it becomes energetically favorable to form more negatively charged B<sup>(4)</sup> units than are needed for compensating all charges of alkali ions. The additional negative charges of B<sup>(4)</sup> units are compensated by the positive charges of P<sup>(4)</sup> units.

The P<sup>(4)</sup> units should have small formation enthalpies also due to their high charge delocalization and their large number of four bOs. One can imagine mutually linked B<sup>(4)</sup> and P<sup>(4)</sup> units to form small crystalline-type cluster configurations, as sketched in Fig. 12 of Ref. 28. The theoretical modeling in Ref. 14 is thus extended by the following additional requirement: *The number of B<sup>(4)</sup> units is maximal under consideration of positively charged P<sup>(4)</sup> units and the constraints given by the stoichiometry, charge neutrality and forbidden B<sup>(4)</sup>-B<sup>(4)</sup> linkages.* For the same reasons as for the B<sup>(4)</sup> units, we expect also that P<sup>(4)</sup> units do not link to themselves. One can check that this further constraint can

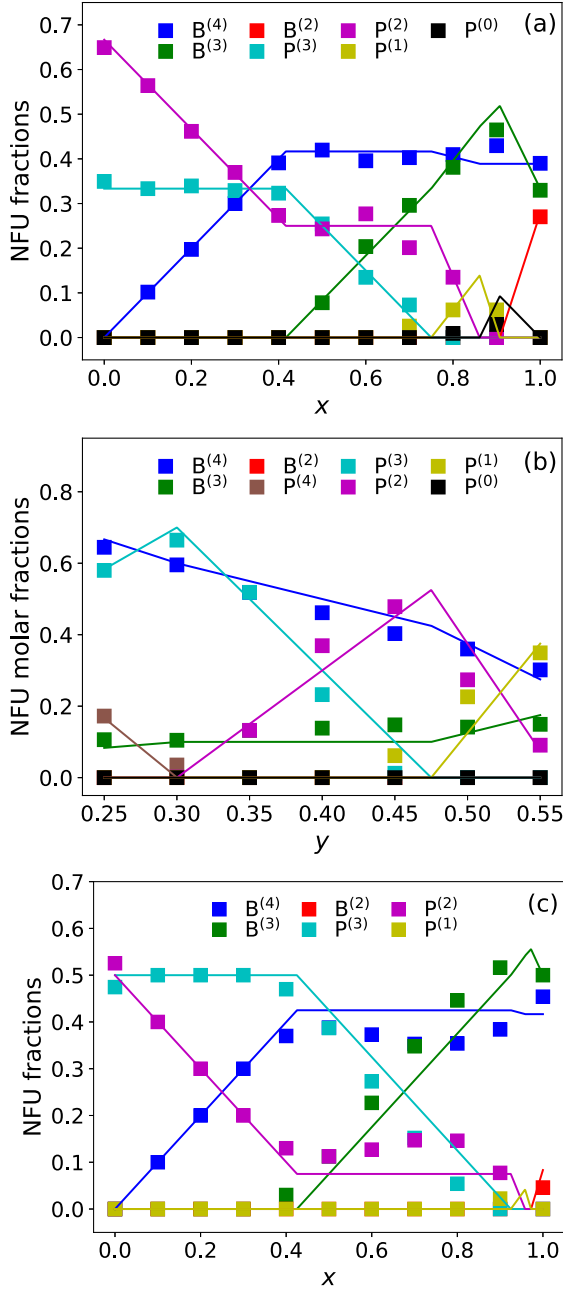


Figure 2: Predicted NFU fractions from Table 1 (solid lines) in comparison with experimental MAS-NMR data (filled squares) for various borophosphate glasses: (a) Glasses with compositions  $0.4\text{Na}_2\text{O}-0.6[x\text{B}_2\text{O}_3-(1-x)\text{P}_2\text{O}_5]$  with experimental data from Ref. 20 for  $0 \leq x \leq 0.9$  and from Ref. 29 for  $x = 1$ ; (b) Glasses with compositions  $y\text{Na}_2\text{O}-2(1-y)[\text{BPO}_4]$  with experimental data from Ref. 28. For  $x = 0.25$ , the theoretical values with consideration of  $\text{P}^{(4)}$  units were used (see text); (c) Glasses with compositions  $0.33\text{Li}_2\text{O}-0.67[x\text{B}_2\text{O}_3-(1-x)\text{P}_2\text{O}_5]$  with experimental data from Ref. 27.

always be fulfilled with the NFU fractions calculated below.

The requirement of forbidden  $\text{B}^{(4)}\text{-B}^{(4)}$  linkages implies

$$4\{\text{B}^{(4)}\} \leq 3\{\text{B}^{(3)}\} + 2\{\text{B}^{(2)}\} + 4\{\text{P}^{(4)}\} + 3\{\text{P}^{(3)}\} + 2\{\text{P}^{(2)}\} + \{\text{P}^{(1)}\} \quad (4)$$

Using this relation, the hierarchy of formation enthalpies and the principle of maximal possible number of  $\text{B}^{(4)}$  units, we predict four different regimes 1 to 4 to occur for  $\{M\} \leq \{M\}_*$ , where certain NFU types are replaced by certain other types. Refinements are possible by considering disproportionation reactions but we are not including them in the following analysis. The four regimes are as follows:

*Regime 1* ( $0 \leq x \leq x_1$ ): *Replacement of  $\text{P}^{(2)}$  by  $\text{B}^{(4)}$  units.* In the phosphate glass ( $x = 0$ ), the charges of the alkali ions are compensated by the  $\text{P}^{(2)}$  units,  $\{\text{P}^{(2)}\} = \{M\}$  and the rest of the network is formed by the neutral  $\text{P}^{(3)}$  units,  $\{\text{P}^{(3)}\} = 1 - \{M\}$ . When  $x$  is increased,  $\text{P}^{(2)}$  are first replaced by  $\text{B}^{(4)}$  units, because  $\text{B}^{(4)}$  is the most favorable NFU type for charge compensation (smallest formation enthalpy of the negatively charged NFU types). The fraction of  $\text{P}^{(3)}$  units does not change. Equations (2a)-(2c) then yield

$$\{\text{B}^{(4)}\} = x, \quad (5a)$$

$$\{\text{P}^{(2)}\} = \{M\} - x, \quad (5b)$$

$$\{\text{P}^{(3)}\} = 1 - \{M\}. \quad (5c)$$

The regime terminates when all  $\text{P}^{(2)}$  units are substituted at

$$x_1 = \{M\}. \quad (6)$$

One can easily check that the constraint in Eq. (4) is always fulfilled for the fractions in Eqs. (5a)-(5c) if  $\{M\} \leq \{M\}_*$ .

*Regime 2* ( $x_1 \leq x \leq x_2$ ): *Replacement of  $\text{P}^{(3)}$  by  $\text{P}^{(4)}$  and  $\text{B}^{(4)}$  units.* According to the discussion above, more negatively charged  $\text{B}^{(4)}$  units can form than are needed for compensating the alkali ion charges. This holds true as long as  $\text{B}^{(4)}\text{-B}^{(4)}$  linkages can be avoided. The addi-

tional negative charges of  $B^{(4)}$  units are compensated by the positive charges of  $P^{(4)}$  units. The network is now formed by  $B^{(4)}$ ,  $P^{(3)}$  and  $P^{(4)}$  units and Eqs. (2a)-(2c) yield

$$\{B^{(4)}\} = x, \quad (7a)$$

$$\{P^{(3)}\} = 1 + \{M\} - 2x, \quad (7b)$$

$$\{P^{(4)}\} = x - \{M\}. \quad (7c)$$

This regime terminates, if condition (4) becomes violated at

$$x_2 = \frac{1}{2} - \frac{\{M\}}{6}, \quad (8)$$

i.e. when  $B^{(4)}$ - $B^{(4)}$  linkages can no longer be avoided. For  $\{M\} = \{M\}_* = 3/7$  in particular, it holds  $x_2 = x_1$  and the regime 2 disappears. This explains why we expect  $P^{(4)}$  units to be absent for  $\{M\} \geq \{M\}_*$ .

*Regime 3* ( $x_2 \leq x \leq x_3$ ): *Replacement of  $P^{(3)}$  by  $B^{(3)}$  units.* As the fraction of  $B^{(4)}$  units has saturated,  $B^{(3)}$  units are replacing  $P^{(3)}$  units now. The network is formed by  $B^{(3)}$ ,  $B^{(4)}$ ,  $P^{(3)}$ , and  $P^{(4)}$  units. Equations (2a)-(2c) together with condition (4) (as equation) yield

$$\{B^{(3)}\} = -\frac{1}{2} + \frac{1}{6}\{M\} + x, \quad (9a)$$

$$\{B^{(4)}\} = \frac{1}{2} - \frac{1}{6}\{M\}, \quad (9b)$$

$$\{P^{(3)}\} = \frac{1}{2} + \frac{7}{6}\{M\} - x, \quad (9c)$$

$$\{P^{(4)}\} = \frac{1}{2} - \frac{7}{6}\{M\}. \quad (9d)$$

The regime terminates when all  $P^{(3)}$  units are replaced at

$$x_3 = \frac{1}{2} + \frac{7}{6}\{M\}. \quad (10)$$

*Regime 4* ( $x_3 \leq x \leq x_4$ ): *Replacement of  $P^{(4)}$  by  $B^{(3)}$  units.* Eventually  $B^{(3)}$  units replace  $P^{(4)}$  units and the number of  $B^{(4)}$  units decreases to keep the overall charge neutrality. The network is formed by  $B^{(3)}$ ,  $P^{(4)}$  and  $B^{(4)}$  units and

Eqs. (2a)-(2c) yield

$$\{B^{(3)}\} = -1 - \{M\} + 2x, \quad (11a)$$

$$\{B^{(4)}\} = 1 + \{M\} - x, \quad (11b)$$

$$\{P^{(4)}\} = 1 - x. \quad (11c)$$

This behaviour continues until at  $x = 1$  the network is built by charged  $B^{(4)}$  units with fraction  $\{B^{(4)}\} = \{M\}$  and neutral  $B^{(3)}$  units with fraction  $\{B^{(3)}\} = 1 - \{M\}$ .

The predicted variations of the fractions of NFU types in the four regimes 1-4 are summarized in Table 2. A few experimental results for NFU fractions when  $\{M\} < \{M\}_* = 3/7$ , or  $y < 0.3$ , are shown in Fig. 2(b). They are in good agreement with the theoretical predictions.

### 3 Site Energy Landscapes for Charge Transport

The negatively charged NFUs form counter charges for the mobile alkali ions. If the relative concentrations of NFU types change, the spatial distribution of the counter charge becomes modified and hence the energy landscape for the ion migration. To describe changes of conductivity activation energies  $E_a$  with the glass composition in alkali borophosphate glasses, we base our modeling on the hypothesis that the modification of site energies, i.e. the energies of the mobile ions at their residence sites in the glass network, plays the decisive role.

In general, when considering a jump of a mobile ion from a site  $i$  to a vacant neighboring site  $j$ , the energies  $\tilde{\epsilon}_i$  and  $\tilde{\epsilon}_j$  of the ion at the initial and target site matter,<sup>1</sup> as well as the saddle point energy to be surmounted. All these energies are affected by the NFUs in the environment of the sites  $i, j$  and by the Coulomb interaction with the other mobile ions. To assume that the NFU contribution to the site energies is decisive, requires the spatial variation of the

<sup>1</sup>The notation with the tilde is used, because we analyze the charge transport finally in a vacancy picture, where the vacancies have site energies  $\epsilon_i = -\tilde{\epsilon}_i$ , see below.

$\tilde{\epsilon}_i$  caused by the Coulomb contribution to be weak compared to that caused by the NFUs. In addition, the saddle point energies should vary weakly in comparison to the site energies.

As for the Coulomb interaction, molecular dynamics simulations suggest that the assumption of a weakly fluctuating contribution to the energetics of ion jumps is better justified in a “vacancy picture”.<sup>32–34</sup> In this picture, one considers the vacancies, i.e. the vacant ion sites as charge carriers with a negative charge (analogous to hole conduction in energy bands of semiconductors). Only a small fraction  $f_0$  of the ion sites is found to be vacant in molecular dynamics simulations, with  $f_0$  typical in the range of 3-10%.<sup>35–38</sup> Small vacancy concentrations can be expected on thermodynamic reasons, because “defect concentrations” should be small in melt-grown glasses.<sup>39</sup> It was furthermore shown that  $f_0 \ll 1$  is required to understand the peculiar behavior seen in the internal friction behavior of mixed alkali glasses.<sup>40,41</sup>

To construct site energy landscapes in alkali borophosphate glasses, we follow the approach in Ref. 14 and consider the two simple-cubic sublattices of a body-centered cubic lattice. A two-dimensional sketch of these sublattices is shown in Fig. 3. One of the sublattices is the “NFU lattice”. Its “NFU sites” are randomly occupied by NFUs of different types, where each type occurs with its respective concentration.

On the other sublattice, termed the “M lattice”, we consider the ionic motion to take place. A site in this M lattice can be occupied by at most one mobile ion and ionic motion proceeds by jumps of ions to vacant nearest neighbor site (as long these are accessible, see below). As the amount of mobile ions relative to the total number of NFUs is  $\{M\} = y/(1-y)$  (see Sec. 2), a fraction  $y/(1-y)$  of all sites in the M lattice is occupied. This requires  $\{M\} = y/(1-y) < 1$ , meaning that the applicability of the method is restricted to glass compositions with  $y < 1/2$ . It is possible to introduce other types of interwoven sublattices to lift this restriction. As we consider compositions with  $y = 0.33$  and  $y = 0.4$  in Sec. 4 below, corresponding refinements of the approach are not necessary here.

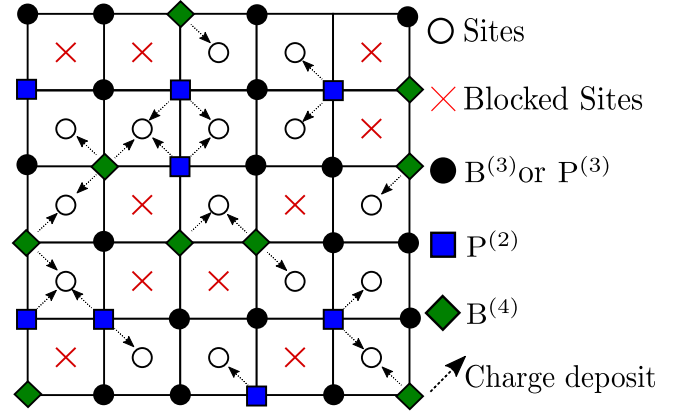


Figure 3: Two-dimensional sketch illustrating the M sublattice with accessible ion sites (open circles) and blocked sites (crosses), and the NFU sublattice with sites randomly occupied by different NFUs (with the different species occurring with their respective concentrations). The arrows indicate how the charge of the NFUs (see also Fig. 1) is distributed among the neighboring ion sites.

As for the remaining fraction of unoccupied sites in the M lattice, not all of these sites are considered to be accessible for the mobile ions. This is because the corresponding fraction of vacant sites would be too high (51% for  $y = 0.33$  and 33% for  $y = 0.4$ ). In the modeling, we fix the fraction  $f_0$ , i.e. the number of vacant sites relative to the number of accessible residence sites. All remaining unoccupied sites in the M lattice are blocked. The fraction of blocked sites (relative to all sites in the M lattice) is then given by

$$f_{bl} = 1 - \frac{1}{1 - f_0} \frac{y}{1 - y}. \quad (12)$$

To summarize, for a given  $f_0$  in the range 3-10%, we block a fraction  $f_{bl}$  of sites in the M lattice according to Eq. (12). The other sites are the accessible residence sites, which we refer to as “ion sites” in the following.<sup>2</sup>

To the ion sites are assigned partial charges in dependence of the surrounding neighboring NFUs in the NFU lattice, where we take into

<sup>2</sup>It is possible that finite clusters of ion sites arise due to the blocking, which are not connected to the percolating cluster of ion sites.

account how charge is localized in the different NFU types (see the red circles in Fig. 1). The procedure is illustrated by the arrows in Fig. 3.

Consider an NFU of type  $\alpha$  with charge  $q_\alpha$  and  $k_\alpha$  nbOs that occupies an NFU site, which has  $z$  ion sites in its immediate surroundings. This means that  $z$  of its 8 nearest neighbor sites in the M lattice are accessible for the mobile ions. Among these  $z$  ion sites, we select  $k_\alpha$  randomly and add a partial charge  $q_\alpha/k_\alpha$  to them (in the rare case  $z < k_\alpha$ , the NFU is interchanged with a charge-neutral one at another site; all charges of the NFUs can then be distributed as described). For a negatively charged  $B^{(4)}$  unit without nbO, where the charge  $q_{B^{(4)}} = -1$  can be viewed as delocalized over all four oxygens, we add a charge  $(-1/z)$  uniformly to all surrounding ion sites. A  $P^{(4)}$  unit with  $q_{P^{(4)}} = +1$  would be treated analogously, but for  $y = 0.33$  and  $y = 0.4$ , we have  $\{M\} > 3/7$  and  $P^{(4)}$  units do not appear (see Sec. 2).

All partial charges at an ion site  $i$  are summed up to the total charge

$$Q_i = \sum_{j(i)} q_j. \quad (13)$$

where the sum over  $j = j(i)$  runs over all eight NFU sites  $j$  surrounding the ion site  $i$ , and  $q_j$  is the partial charge contribution of the NFU at site  $j$  ( $q_j = 0$  if the NFU at site  $j$  is charge-neutral).

The total charge  $Q_i$  gives rise to a site energy

$$\tilde{\epsilon}_i^{(0)} = V_0 Q_i, \quad (14)$$

where  $V_0$  is an energy scale. This scale can be roughly estimated by the Coulomb interaction between an alkali ion with positive charge and an oxygen with negative charge at a distance of about  $2\text{\AA}$ . The precise value  $V_0$ , however, is not relevant, when we consider relative changes of activation energies with the glass composition in Sec. 4.

To account for additional structural and energetic disorder, we add fluctuations  $V_0\eta_i$  to the sites energies, where the  $\eta_i$  are uncorrelated Gaussian random numbers with zero mean and

standard deviation  $\sigma_\epsilon$ ,

$$\tilde{\epsilon}_i = \tilde{\epsilon}_i^{(0)} + V_0\eta_i = V_0(Q_i + \eta_i). \quad (15)$$

The fluctuations have several sources. In particular they should take into consideration that sites in a glass are not located on a simple cubic lattice, and that there is an additional contribution from the Coulomb interaction between mobile ions (see the discussion above). Moreover, for ion jump rates, whose variation depends only on the site energies, we can think of the fluctuations to take into account also spatial variations of the saddle points energies.

As the structure of the glass changes with the borate to phosphate mixing ratio, the standard deviation or “disorder parameter”  $\sigma_\epsilon$  should depend on  $x$  also. However, according to our hypothesis, the redistribution of counter-charges and associated modifications of the site energies should be the main cause of changes in long-range ion transport properties. Hence,  $\sigma_\epsilon$  should vary only weakly with  $x$ . More precisely, its variation with  $x$  should be small compared to the variations of the  $\tilde{\epsilon}_i^{(0)}$  in Eq. (14). In order to see whether the dependence of conductivity activation energies  $E_a$  on  $x$  can be captured without adjusting  $\sigma_\epsilon$  for each  $x$ , we deliberately constrain  $\sigma_\epsilon$  to a fixed value. It is the only fit parameter then, when we calculate normalized values  $E_a(x)/E_a(0)$  for different mixing ratios  $x$  in the next section.

## 4 Conductivity Activation Energies

In a former study,<sup>14</sup> it was shown that the change of  $E_a(x)/E_a(0)$  with  $x$  in the glasses  $0.4\text{Na}_2\text{O}-0.6[x\text{B}_2\text{O}_3-(1-x)\text{P}_2\text{O}_5]$  could be successfully modeled based on the energy landscape construction presented in Sec. 3, despite of its simplicity. The activation energies in the respective study were obtained by extensive kinetic Monte-Carlo (KMC-) simulations with a Metropolis form of the jump rates of the mobile ions for  $f_0 = 0.1$ . Using a disorder parameter  $\sigma_\epsilon = 0.3$ , good agreement with measured values was obtained, see the filled (experiment)



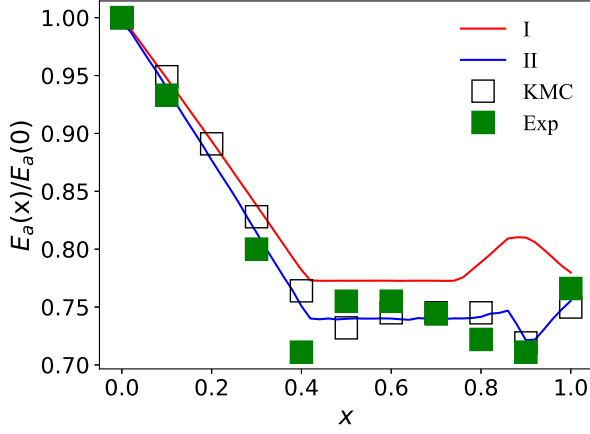


Figure 4: Normalized activation energy  $E_a(x)/E_a(0)$  as a function of the network former mixing ratio  $x$  in sodium borophosphate glasses with compositions  $0.4\text{Na}_2\text{O}-0.6[x\text{B}_2\text{O}_3-(1-x)\text{P}_2\text{O}_5]$ . The filled symbols are experimental data taken from Ref. 20 and the open symbols results from KMC simulations reported in Ref. 14, the value at  $x = 1$  obtained from the KMC simulations has been recalculated. The lines correspond to the analytically calculated activation energies from approaches I (red line) and II (blue line).

and open (KMC simulations) symbols in Fig. 4. The energy scale  $V_0$  in real units can be estimated by requiring the measured value  $E_a(0)$  to agree with the simulated one. This yields  $V_0 \simeq 1.29 \text{ eV}$ .

Here we will present two analytical approaches I and II to determine the activation energy and compare the results to those obtained earlier by the KMC simulations. Approach II will be applied also to lithium borophosphate glasses with compositions  $0.33\text{Li}_2\text{O}-0.67[x\text{B}_2\text{O}_3-(1-x)\text{P}_2\text{O}_5]$ . For both analytical approaches we use the vacancy picture, for which the site energies  $\epsilon_i$  have opposite sign,  $\epsilon_i = -\tilde{\epsilon}_i$ .

Method I is based on a simple picture that has been used in former works.<sup>24,42</sup> It is illustrated in Fig. 5, where we show the distribution of site energies resulting from our landscape construction for the glass  $0.4\text{Na}_2\text{O}-0.6[x\text{B}_2\text{O}_3-(1-x)\text{P}_2\text{O}_5]$  with  $x = 0.25$ . In the low-temperature limit  $T \rightarrow 0$ , the vacancies fill up all sites with energies  $\epsilon_i < \epsilon_f$ , where  $\epsilon_f$

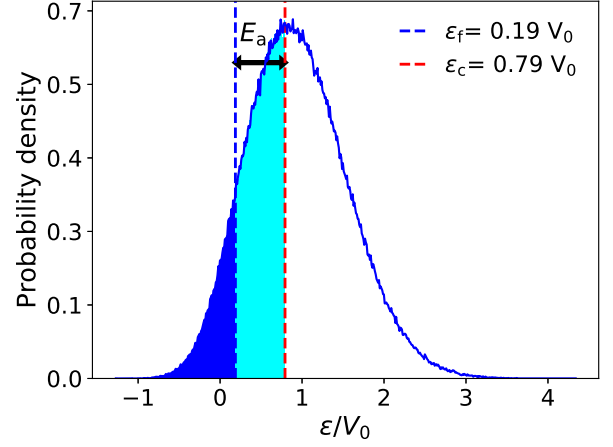


Figure 5: Distribution of site energies for vacancies according to the energy landscape construction described in Sec. 3 for the glass  $0.4\text{Na}_2\text{O}-0.6[x\text{B}_2\text{O}_3-(1-x)\text{P}_2\text{O}_5]$  with  $x = 0.25$ . The fraction of vacancies relative to all accessible sites is  $f_0 = 0.1$ . The Fermi energy  $\epsilon_f$  indicates the highest energy of vacant sites in thermal equilibrium in the low temperature limit  $T \rightarrow 0$ . The critical energy  $\epsilon_c$  is the minimal site energy required for all sites with  $\epsilon_i \leq \epsilon_c$  to form a percolating path. The difference  $(\epsilon_c - \epsilon_f)$  gives the activation energy  $E_a$  in model I.

is the Fermi energy.<sup>3</sup> Due to thermal fluctuations, vacancies can move through the “whole system” (long range diffusion corresponding to dc-conductivity), where at low temperatures the respective diffusion path should consist of all sites with energies  $\epsilon_i$  below a critical value  $\epsilon_c$ . This critical value is the lowest one, where a connected path of sites with energies below a given threshold  $\epsilon_{\text{th}}$  can form, i.e.  $\epsilon_c = \min_{\epsilon_{\text{th}}}(\text{set of sites with } \epsilon_i \leq \epsilon_{\text{th}} \text{ is percolating})$ . The conductivity activation energy is then given by

$$E_a = \epsilon_c - \epsilon_f. \quad (16)$$

We have determined both the Fermi energy  $\epsilon_f$  and the critical energy  $\epsilon_c$  by generating site energy landscapes in systems (M lattices) with  $100^3$  sites. The determination of  $\epsilon_f$  is straightforward and for determining the critical energy  $\epsilon_c$  we used the Hoshen-Kopelman algorithm of

<sup>3</sup>Note that a site can be occupied by at most one vacancy, i.e. the Fermi statistics applies to the vacancies as well.

percolation theory.<sup>43</sup> Once the algorithm is implemented, the calculation of one value of  $E_a$  takes just a few minutes on a standard personal computer.

The normalized  $E_a(x)/E_a(0)$  calculated for the glasses  $0.4\text{Na}_2\text{O}-0.6[x\text{B}_2\text{O}_3-(1-x)\text{P}_2\text{O}_5]$  with approach I is shown in Fig. 4 (red line) for the fixed value  $f_0 = 0.1$  formerly used in the KMC simulations. The agreement with the KMC results (open symbols) is good for  $x \lesssim 0.3$ , but for larger mixing ratios the activation energy is overestimated. At  $x \cong 0.9$ , the predicted  $E_a(x)$  exhibits a local maximum, while the KMC results indicate a local minimum. Hence, model I does not give a satisfactory prediction of  $E_a(x)$  for all  $x$ .

In approach II, we make use of the fact that the hopping transport in a Fermionic lattice gas with site energy disorder can be mapped onto an effective single particle hopping model in a landscape, where all site energies are equal, and the energetic disorder is completely transferred to the jump barriers (this model corresponds also to a random conductance network).<sup>25</sup> The barrier  $\Delta_{ij}$  for a jump from site  $i$  to a nearest-neighbor site  $j$  is given by

$$\Delta_{ij} = \frac{1}{2} (|\epsilon_i - \epsilon_j| + |\epsilon_i - \epsilon_f| + |\epsilon_j - \epsilon_f|) . \quad (17)$$

Note that the barriers are symmetric,  $\Delta_{ij} = \Delta_{ji}$ , and that the vacancy concentration enters via the Fermi energy  $\epsilon_f$ . Bonds in the M lattice connected to blocked sites are assigned infinite barriers.

The activation energy follows by considering all bonds  $(ij)$  with  $\Delta_{ij}$  below a threshold value  $\Delta_{\text{th}}$ . It holds

$$E_a = \Delta_c , \quad (18)$$

where  $\Delta_c$  is the critical smallest value of the thresholds, where the bonds with  $\Delta_{ij} \leq \Delta_{\text{th}}$  still form a percolating path, i.e.  $\Delta_c = \min_{\Delta_{\text{th}}}(\text{set of bonds } (ij) \text{ with } \Delta_{ij} \leq \Delta_{\text{th}} \text{ is percolating})$ .

Figure 6 shows as an example the distribution of barriers calculated from Eq. (17) for the same energy landscape used in Figure 5. The critical barrier  $\Delta_c$  indicated by the red vertical line was determined again by using the Hoshen-

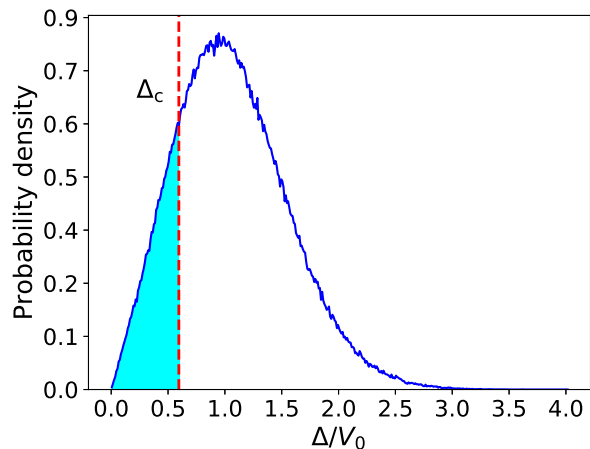


Figure 6: Distribution of energy barriers calculated from the site energies according to Eq. (17) for the same energy landscape as considered in Fig. 5. The critical barrier  $\Delta_c$  is the minimal barrier energy required for all bonds with  $\Delta_{ij} \leq \Delta_c$  to form a percolating path. It equals the activation energy  $E_a$ .

Kopelman algorithm, where this time the bond percolation was evaluated.

The activation energies from approach II are shown in Fig. 4 as blue line and agree well with the KMC results for all mixing ratios  $x$ . Small deviations can be attributed to uncertainties in the  $E_a$  values calculated from the KMC simulations. Hence, conductivity activation energies can now be calculated very quickly without the need to perform extensive KMC simulations for various temperatures and subsequently extracting  $E_a$  from Arrhenius plots.

Let us apply the procedure to another series of alkali borophosphate glasses, namely the lithium conducting ones with compositions  $0.33\text{Li}_2\text{O}-0.67[x\text{B}_2\text{O}_3-(1-x)\text{P}_2\text{O}_5]$ . Experimental results for NFU concentrations (see Fig. 2) and conductivity activation energies for these glasses were reported in Ref. 27. To construct site energy landscapes for them, we take two fixed values  $f_0 = 0.05$  and  $f_0 = 0.1$  of the vacancy fraction in order to see, whether the specific value of  $f_0$  is important. To determine the disorder parameter  $\sigma_\epsilon$ , we require  $E_a(1)/E_a(0)$  to match the experimental value for each of the two considered  $f_0$  values. This means that  $\sigma_\epsilon$  is solely determined by the phosphate ( $x = 0$ ) and borate ( $x = 1$ ) glass. The variation of

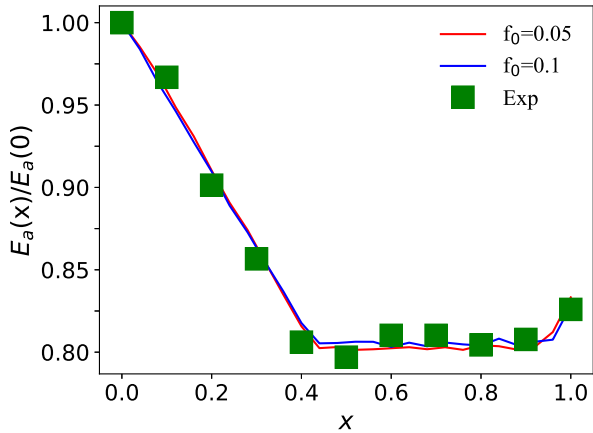


Figure 7: Normalized activation energy  $E_a(x)/E_a(0)$  as a function of the network former mixing ratio  $x$  in lithium borophosphate glasses with compositions  $0.33\text{Li}_2\text{O}-0.67[x\text{B}_2\text{O}_3-(1-x)\text{P}_2\text{O}_5]$ . The filled symbols are experimental data taken from Ref. 27 and the lines analytically calculated activation energies with approach II based on the energy landscape construction described in Sec. 3 for  $f_0 = 0.05$  (red line) and  $f_0 = 0.1$  (blue line). The disorder parameter (standard deviation)  $\sigma_\epsilon$  for the Gaussian fluctuations in Eq. (15) was chosen to match the experimental value  $E_a(1)/E_a(0)$  ( $\sigma_\epsilon = 0.44$  for  $f_0 = 0.05$  and  $\sigma_\epsilon = 0.49$  for  $f_0 = 0.1$ ).

$E_a(x)/E_a(0)$  with the network former mixing ratio is then a prediction of the theoretical modeling, i.e. not affected by any parameter fitting.

We find  $\sigma_\epsilon = 0.44$  for  $f_0 = 0.05$  and a slightly larger value  $\sigma_\epsilon = 0.49$  for  $f_0 = 0.1$ . The predicted behavior for  $E_a(x)/E_a(0)$  as a function of  $x$  (red line for  $f_0 = 0.05$ , blue line for  $f_0 = 0.1$ ) is shown in Fig. 7 and compares very well with the measured data (symbols). When calculating  $V_0$  in real units by requiring the measured value  $E_a(0)$  to agree with the simulated one, we obtain the estimates  $V_0 \simeq 0.69\text{ eV}$  for  $f_0 = 0.05$  and  $V_0 \simeq 0.80\text{ eV}$  for  $f_0 = 0.1$ . Let us note that we checked also the robustness against changes of  $f_0$  in our modeling of the sodium borophosphate glasses considered in Fig. 4.

## 5 Summary and Conclusions

For alkali borophosphate glasses, we derived analytical results for NFU concentrations, constructed site energy landscapes based on the concentrations and charges of the NFUs, and calculated conductivity activation energies from these landscapes by applying a method, which requires only a simple and quick determination of Fermi and critical percolation energies. The results for the predicted NFU concentrations and activation energies compare well with experimental data. We thus regard our theoretical approach as a promising step forward toward relating structure to transport properties in ionically conducting glasses, and toward developing a theoretical understanding of ion transport in glasses with quantitative predictive power.

There is plenty of room for further developments of the approach. One important refinement will be to incorporate spatial correlations between the NFUs of the various types in the energy landscape construction. These spatial correlations can be measured, for example, by applying dipolar recoupling methods in rotational-echo double-resonance (REDOR) measurements of advanced solid state NMR<sup>27,28,44,45</sup> (for a recent review of solid state NMR studies on borophosphate glasses, see Ref. 46). Another point is to evaluate aspects of the constructed energy landscapes more directly with respect to experimental observations, as, for example, those obtained from the recently developed method of charge attachment induced transport (CAIT).<sup>47,48</sup> Further improvements concern a more detailed modeling of the local jump dynamics with explicit consideration of saddle point energies and disorder in the spatial arrangements of ion sites.

The mapping of the (many-body) jump model with varying site energies to a single particle model with varying jump barriers moreover provides insights, why the random barrier model<sup>49,50</sup> is successful to capture the quasi-universal scaling behavior of conductivity spectra in glasses with one type of mobile ion.<sup>51-53</sup> A

corresponding mapping is not possible if more than one type of mobile ion is present, as, e.g., in mixed alkali glasses. One may thus expect that conductivity scaling in such glasses is not observed, which is indeed the case.<sup>54</sup> Calculations of conductivity spectra and preexponential factors of dc conductivities will be presented in upcoming work.

**Acknowledgement** P.M. thanks H. Eckert and S. W. Martin for very valuable discussions. This work has been funded by the Deutsche Forschungsgemeinschaft (DFG, Project No. 428906592). We sincerely thank the members of the DFG Research Unit FOR 5065 for fruitful discussions.

## References

- (1) Ingram, M. D. Ionic Conductivity in Glass. *Phys. Chem. Glasses* **1987**, *28*, 215–234.
- (2) Dyre, J. C.; Maass, P.; Roling, B.; Sidebottom, D. L. Fundamental questions relating to ion conduction in disordered solids. *Rep. Prog. Phys.* **2009**, *72*.
- (3) Hakim, R. M.; Uhlmann, D. R. Electrical conductivity of alkali silicate glasses. *Phys. Chem. Glasses* **1971**, *12*, 132–138.
- (4) Kawamura, J.; Shimoji, M. Glass transition and ac conductivity of  $\text{Ag}^+$  conducting glasses. *Mater. Chem. Phys.* **1989**, *23*, 99 – 120.
- (5) Deshpande, V. K.; Pradel, A.; Ribes, M. The mixed glass former effect in the  $\text{Li}_2\text{S} : \text{SiS}_2 : \text{GeS}_2$  system. *Materials Research Bulletin* **1988**, *23*, 379 – 384.
- (6) Jayasinghe, G.; Bandaranayake, P.; Souquet, J. Mixed former effect in sodium phospho tellurate glasses. *Solid State Ionics* **1996**, *86-88*, 447 – 451.
- (7) Anderson, O. L.; Stuart, D. A. Calculation of activation energy of ionic conductivity in silica glasses by classical methods. *J. Am. Ceram. Soc.* **1954**, *37*, 573–580.
- (8) Maass, P.; Bunde, A.; Ingram, M. D. Ion transport anomalies in glasses. *Phys. Rev. Lett.* **1992**, *68*, 3064–3067.
- (9) Hunt, A. New Developments in the theory of the hopping conductivity of spatially random systems. *J. Phys.: Condens. Matter* **1994**, *6*, 1239–1252.
- (10) Maass, P. Towards a theory for the mixed alkali effect in glasses. *J. Non-Cryst. Solids* **1999**, *255*, 35–46.
- (11) Adams, S.; Swenson, J. Determining Ionic Conductivity from Structural Models of Fast Ionic Conductors. *Phys. Rev. Lett.* **2000**, *84*, 4144–4147.
- (12) Pradel, A.; Kuwata, N.; Ribes, M. Ion transport and structure in chalcogenide glasses. *J. Phys. Condens. Matter* **2003**, *15*, S1561–S1571.
- (13) Schuch, M.; Mueller, C. R.; Maass, P.; Martin, S. W. Mixed Barrier Model for the Mixed Glass Former Effect in Ion Conducting Glasses. *Phys. Rev. Lett.* **2009**, *102*.
- (14) Schuch, M.; Trott, C.; Maass, P. Network forming units in alkali borate and borophosphate glasses and the mixed glass former effect. *RSC Adv.* **2011**, *1*, 1370–1382.
- (15) Wang, W.; Christensen, R.; Curtis, B.; Martin, S. W.; Kieffer, J. A new model linking elastic properties and ionic conductivity of mixed network former glasses. *Phys. Chem. Chem. Phys.* **2018**, *20*, 1629–1641.
- (16) Haynes, M. J.; Bischoff, C.; Kaufmann, T.; Martin, S. W. The Mixed Glass Former Effect on the Thermal and Volume Properties of  $\text{Na}_2\text{S}-\text{B}_2\text{S}_3-\text{P}_2\text{S}_5$  Glasses. *Phys. Chem. Glasses: Eur. J. of Glass Science and Technol. Part B* **2009**, *50*, 144–148.
- (17) Martin, S. W.; Bischoff, C.; Schuller, K. Composition Dependence of the  $\text{Na}^+$  Ion

- Conductivity in  $0.5\text{Na}_2\text{S}+0.5x\text{GeS}_2+(1-x)\text{PS}_{5/2}$  Mixed Glass Former Glasses: A Structural Interpretation of a Negative Mixed Glass Former Effect. *J. Phys. Chem. B* **2015**, *119*, 15738–15751.
- (18) Martin, S. W.; Christensen, R.; Olson, G.; Kieffer, J.; Wang, W. New Interpretation of Na<sup>+</sup>-Ion Conduction in and the Structures and Properties of Sodium Borosilicate Mixed Glass Former Glasses. *J. Phys. Chem. C* **2019**, *123*, 5853–5870.
- (19) Anantha, P. S.; Hariharan, K. Structure and ionic transport studies of sodium borophosphate glassy system. *Mater. Chem. Phys.* **2005**, *89*, 428–437.
- (20) Zielniok, D.; Cramer, C.; Eckert, H. Structure Property Correlations in Ion-Conducting Mixed-Network Former Glasses: Solid-State NMR Studies of the System  $\text{Na}_2\text{O}-\text{B}_2\text{O}_3-\text{P}_2\text{O}_5$ . *Chem. Mat.* **2007**, *19*, 3162–3170.
- (21) Schuch, M.; Christensen, R.; Trott, C.; Maass, P.; Martin, S. W. Investigation of the Structures of Sodium Borophosphate Glasses by Reverse Monte Carlo Modeling to Examine the Origins of the Mixed Glass Former Effect. *J. Phys. Chem. C* **2012**, *116*, 1503–1511.
- (22) Karlsson, M.; Schuch, M.; Christensen, R.; Maass, P.; Martin, S. W.; Imberti, S.; Matic, A. Structural Origin of the Mixed Glass Former Effect in Sodium Borophosphate Glasses Investigated with Neutron Diffraction and Reverse Monte Carlo Modeling. *J. Phys. Chem. C* **2015**, *119*, 27275–27284.
- (23) Maass, P.; Meyer, M.; Bunde, A.; Dieterich, W. Microscopic explanation of the non-Arrhenius conductivity in glassy fast ionic conductors. *Phys. Rev. Lett.* **1996**, *77*, 1528–1531.
- (24) Kirchheim, R. The mixed alkali effect as a consequence of network density and site energy distribution. *J. Non-Cryst. Solids* **2000**, *272*, 85 – 102.
- (25) Ambegaokar, V.; Halperin, B. I.; Langer, J. S. Hopping Conductivity in Disordered Systems. *Phys. Rev. B* **1971**, *4*, 2612–2620.
- (26) Tyč, S.; Halperin, B. I. Random resistor network with an exponentially wide distribution of bond conductances. *Phys. Rev. B* **1989**, *39*, 877–880.
- (27) Larink, D.; Eckert, H.; Reichert, M.; Martin, S. W. Mixed Network Former Effect in Ion-Conducting Alkali Borophosphate Glasses: Structure/Property Correlations in the System  $[\text{M}_2\text{O}]_{1/3}[(\text{B}_2\text{O}_3)_x(\text{P}_2\text{O}_5)_{1-x}]_{2/3}$  (M=Li, K, Cs). *The Journal of Physical Chemistry C* **2012**, *116*, 26162–26176.
- (28) Rinke, M. T.; Eckert, H. The mixed network former effect in glasses: solid state NMR and XPS structural studies of the glass system  $(\text{Na}_2\text{O})_x(\text{BPO}_4)_{1-x}$ . *Phys. Chem. Chem. Phys.* **2011**, *13*, 6552–6565.
- (29) Michaelis, V. K.; Aguiar, P. M.; Kroeker, S. Probing alkali coordination environments in alkali borate glasses by multinuclear magnetic resonance. *J. Non-Cryst. Solids* **2007**, *353*, 2582 – 2590.
- (30) P. Beekenkamp, in *Physics of Non-Crystalline Solids*, ed. J. A. Prins, North-Holland, Amsterdam, 1965, p. 512.
- (31) Michaelis, V.; Kachhadia, P.; Kroeker, S. Clustering in borate-rich alkali borophosphate glasses: a <sup>11</sup>B and <sup>31</sup>P MAS NMR study. *Phys. Chem. Glasses: Eur. J. Glass Sci. Technol. B* **2013**, *54*, 20–26.
- (32) Vogel, M. Identification of lithium sites in a model of  $\text{LiPO}_3$  glass: Effects of the local structure and energy landscape on ionic jump dynamics. *Phys. Rev. B* **2004**, *70*, 094302.
- (33) Lammert, H.; Banhatti, R. D.; Heuer, A. The cationic energy landscape in alkali silicate glasses: Properties and relevance. *J. Chem. Phys.* **2009**, *131*.

- (34) Lammert, H.; Heuer, A. Simplified Interpretation of Transport in Disordered Inorganic Ion Conductors from Vacancy Dynamics. *Phys. Rev. Lett.* **2010**, *104*, 125901.
- (35) Cormack, A. N.; Du, J.; Zeitler, T. R. Alkali ion migration mechanisms in silicate glasses probed by molecular dynamics simulations. *Phys. Chem. Chem. Phys.* **2002**, *4*, 3193–3197.
- (36) Lammert, H.; Kunow, M.; Heuer, A. Complete Identification of Alkali Sites in Ion Conducting Lithium Silicate Glasses: A Computer Study of Ion Dynamics. *Phys. Rev. Lett.* **2003**, *90*, 215901.
- (37) Habasaki, J.; Hiwatari, Y. Molecular dynamics study of the mechanism of ion transport in lithium silicate glasses: Characteristics of the potential energy surface and structures. *Phys. Rev. B* **2004**, *69*, 144207.
- (38) Müller, C.; Zienicke, E.; Adams, S.; Habasaki, J.; Maass, P. Comparison of ion sites and diffusion paths in glasses obtained by molecular dynamics simulations and bond valence analysis. *Phys. Rev. B* **2007**, *75*.
- (39) Dyre, J. C. Is there a ‘native’ band gap in ion conducting glasses? *J. Non-Cryst. Solids* **2003**, *324*, 192 – 195.
- (40) Peibst, R.; Schott, S.; Maass, P. Internal friction and vulnerability of mixed alkali glasses. *Phys. Rev. Lett.* **2005**, *95*.
- (41) Maass, P.; Peibst, R. Ion diffusion and mechanical losses in mixed alkali glasses. *J. Non-Cryst. Solids* **2006**, *352*, 5178–5187.
- (42) Porto, M.; Maass, P.; Meyer, M.; Bunde, A.; Dieterich, W. Hopping transport in the presence of site-energy disorder: Temperature and concentration scaling of conductivity spectra. *Phys. Rev. B* **2000**, *61*, 6057–6062.
- (43) Hoshen, J.; Kopelman, R. Percolation and cluster distribution. I. Cluster multiple labeling technique and critical concentration algorithm. *Phys. Rev. B* **1976**, *14*, 3438–3445.
- (44) Zhang, L.; Eckert, H. Short- and Medium-Range Order in Sodium Aluminophosphate Glasses: New Insights from High-Resolution Dipolar Solid-State NMR Spectroscopy. *The Journal of Physical Chemistry B* **2006**, *110*, 8946–8958.
- (45) Eckert, H. Spying with spins on messy materials: 60 Years of glass structure elucidation by NMR spectroscopy. *Int. J. Appl. Glass Sci.* **2018**, *9*, 167–187.
- (46) Tricot, G.; Alpysbay, L.; Doumert, B. Solid state NMR: A powerful tool for the characterization of borophosphate glasses. *Molecules* **2020**, *25*, 428.
- (47) Schäfer, M.; Weitzel, K.-M. Site energy distribution of ions in the potential energy landscape of amorphous solids. *Mater. Today Phys.* **2018**, *5*, 12–19.
- (48) Schäfer, M.; Budina, D.; Weitzel, K.-M. Site energy distribution of sodium ions in a sodium rubidium borate glass. *Phys. Chem. Chem. Phys.* **2019**, *21*, 26251–26261.
- (49) Dyre, J. C. The random free-energy barrier model for ac conduction in disordered solids. *J. Appl. Phys.* **1988**, *64*, 2456–2468.
- (50) Dyre, J. C.; Schröder, T. B. Universality of ac conduction in disordered solids. *Rev. Mod. Phys.* **2000**, *72*, 873–892.
- (51) Roling, B.; Happe, A.; Funke, K.; Ingram, M. D. Carrier Concentrations and Relaxation Spectroscopy: New Information from Scaling Properties of Conductivity Spectra in Ionically Conducting Glasses. *Phys. Rev. Lett.* **1997**, *78*, 2160–2163.

- (52) Sidebottom, D. L. Universal Approach for Scaling the ac Conductivity in Ionic Glasses. *Phys. Rev. Lett.* **1999**, *82*, 3653–3656.
- (53) Ghosh, A.; Pan, A. Scaling of the conductivity spectra in ionic glasses: Dependence on the structure. *Phys. Rev. Lett.* **2000**, *84*, 2188–2190.
- (54) Cramer, C.; Brückner, S.; Gao, Y.; Funke, K. Ion dynamics in mixed alkali glasses. *Phys. Chem. Chem. Phys.* **2002**, *4*, 3214–3218.